

Supporting Information

Four-Step Iron(II) Spin State Cascade Driven by Antagonistic Solid State Interactions

Natasha F. Sciortino, Katrina A. Zenere, Maggie E. Corrigan, Gregory J. Halder, Guillaume Chastanet, Jean-François Létard, Cameron J. Kepert and Suzanne M. Neville*

Contents:

S1. Synthesis and Characterisation

S2. Single crystal X-ray diffraction

S3. Powder X-ray diffraction

S4. Magnetic Susceptibility Measurements

S1 Synthesis and Characterisation

All reagents were commercially available and used as received (iron(II) perchlorate was handled carefully and in small amounts to avoid potential explosions). $[\text{Fe}_3(\text{saltrz})_6(\text{Pd/Pt}(\text{CN})_4)_3] \cdot 8(\text{H}_2\text{O})$ (**1^{Pd}**, **1^{Pt}**) crystals were grown by vial-in-vial slow diffusion. Powders of saltrz (22 mg, 0.117 mmol) and $\text{K}_2[\text{Pd}(\text{CN})_4]$ (17 mg, 0.0589 mmol) or $\text{K}_2[\text{Pt}(\text{CN})_4]$ (17 mg, 0.0589 mmol) were placed at the base of a small vial. $\text{Fe}(\text{ClO}_4)_2 \cdot 6(\text{H}_2\text{O})$ (15 mg, 0.0589 mmol) was placed at the base of a large vial. The small vial was placed inside the large vial and both were slowly filled with 50:50 ethanol:water mixture, being careful to fill vials without disturbing the reactants. The components were allowed to diffuse over a period of 2 weeks to form yellow crystals (*ca.* 90% yield). IR(cm^{-1}). **1^{Pd}**: 3573 (br), 3463 (br), 3137 (br), 2745 (br), 2174 (s), 1606 (w), 1524 (m), 1457 (m), 1303 (m), 1267 (m), 1201 (w), 1159 (w), 1059 (s), 762 (w), 539 (w), 417 (w). **1^{Pt}**: 3619 (br), 3137 (br), 2745 (br), 2174 (s), 1607 (m), 1524 (m), 1458 (m), 1303 (m), 1268 (m), 1201 (m), 1160 (m), 1059 (s), 762 (m), 622 (w), 461 (w). CHN analysis was not conducted due to known difficulties in porous materials.

Thermogravimetric analysis on **1^{Pd}** shows a multistep mass loss, whereby the guest water molecules are evolved below 100 °C followed by framework decomposition (Figure S1). The mass loss of *ca.* 6.5% up to 100 °C corresponds with that expected from the material composition $[\text{Fe}_3(\text{saltrz})_6(\text{Pd}(\text{CN})_4)_3] \cdot 8(\text{H}_2\text{O})$ as ascertained by single crystal analysis. The framework is then stable until 200 °C, after which the lattice decomposes in a series of steps.

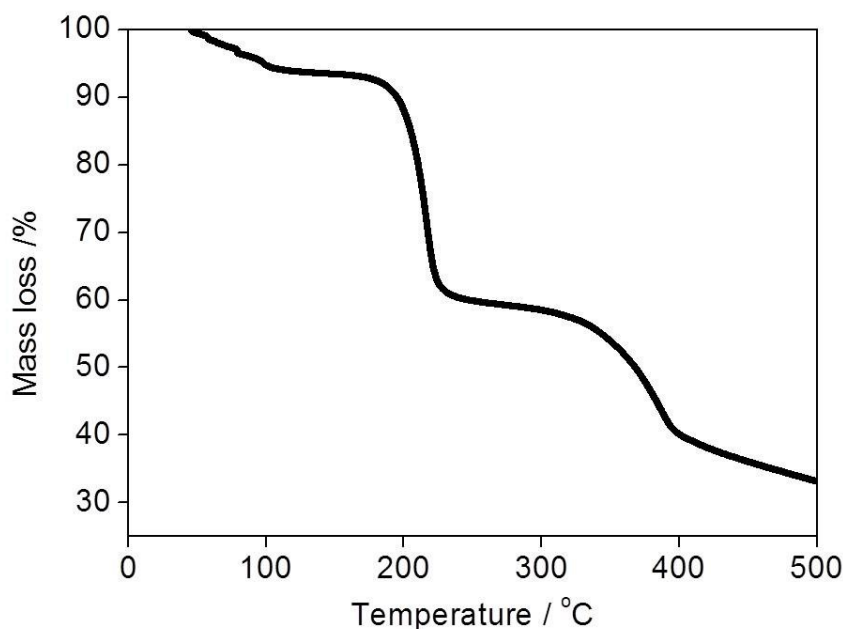


Figure S1. Thermogravimetric analysis of **1^{Pt}** (1 °/min).

S2 Single Crystal X-ray Diffraction

Data were collected on a Bruker APEX diffractometer equipped with a rotating anode ($\lambda = 0.7017 \text{ \AA}$) for **1^{Pt}** and an Agilent SuperNova Dual Source diffractometer employing a Cu-K α radiation source ($\lambda = 1.5418 \text{ \AA}$) for **1^{Pd}**. Data integration and reduction were performed using the Bruker Software suite¹ and CrysAlisPro,² respectively. Structural solution for all materials was completed within SHELXS-97 and refined using SHELXL-97 within the X-SEED user interface.³⁻⁶ All atoms were refined anisotropically and hydrogen atoms were fixed using the riding model.

Single-crystal diffraction data were collected at 240, 192, 170, 120 and 90 K on crystals of **1^{Pt}** (CCDC 1038403-1038407). The single crystal structural refinement parameters and structural details are summarised in Table S1. Variable temperature structural collections were conducted on **1^{Pd}** at a range of temperatures over the spin transition region, resulting in reduced diffraction quality compared to the 230 K structure, so only unit cell parameters could be extracted. This reduced diffraction quality with cooling is also evident in the variable temperature powder X-ray diffraction data. Table S2 reports single crystal refinement details for **1^{Pd}** at 230 K (CCDC 1038408). Selected bond lengths, angles and other parameters for **1^{Pt}** and **1^{Pd}** are listed in Tables S3 - 6. Thermal ellipsoid diagrams (ORTEP 50% probability) for all structures are presented in Figures S2 – 4. Variable temperature procession images for **1^{Pt}** are shown in Figure S5.

Table S1. Single crystal data and refinement details for 1^{Pt}					
Temperature /K	240	192	170	120	90
Spin State, HS ⁿ LS ¹⁻ⁿ	HS ^{1.0} LS ^{0.0}	HS ^{0.833} LS ^{0.167}	HS ^{0.667} LS ^{0.333}	HS ^{0.167} LS ^{0.833}	HS ^{0.0} LS ^{1.0}
Formula, FW /gmol ⁻¹	C ₆₆ H ₄₈ Fe ₃ N ₃₆ O ₁₄ Pt ₃ , 2322.22				
Crystal system	Triclinic (<i>P</i> -1)				
<i>a</i> / Å	10.511(3)	16.409(3)	16.360(3)	10.1859(17)	10.1751(17)
<i>b</i> / Å	13.844(4)	16.433(5)	16.405(6)	13.756(2)	13.735(2)
<i>c</i> / Å	16.456(4)	17.834(3)	17.760(3)	15.908(3)	15.885(3)
α /°	107.906(6)	100.833(6)	101.076(6)	108.017(4)	107.988(4)
β /°	108.092(7)	116.139(4)	116.024(4)	107.260(4)	107.187(4)
γ /°	95.725(6)	95.950(6)	95.939(6)	95.777(4)	95.713(4)
<i>V</i> / Å ³	2114.9(9)	4144.3(17)	4107.0(17)	1978.4(6)	1972.2(6)
ρ_{calc} / Mgm ⁻³	1.823	1.861	1.878	1.949	1.955
data/restraints/parameters	8666/0/553	16859/6/1092	16892/6/1102	8084/0/553	8062/0/548
<i>R</i> (<i>F</i>) { <i>I</i> > 2 σ (<i>I</i>), all} / %	0.0361{0.0540}	0.0661{0.1461}	0.0509{0.0962}	0.0378{0.0578}	0.0380{0.0550}
<i>R</i> _w (<i>F</i> ²) { <i>I</i> > 2 σ (<i>I</i>), all} / %	0.0950{0.1072}	0.1687{0.2237}	0.1214{0.1517}	0.1002{0.1151}	0.1036{0.1159}
GoF	1.049	1.061	1.072	1.090	1.070

Table S2. Single crystal data and refinement details for 1 ^{Pd}	
Temperature /K	230
Spin State, HS ⁿ LS ¹⁻ⁿ	HS ^{1.0} LS ^{0.0}
Formula, FW /gmol ⁻¹	C ₆₆ H ₄₈ Fe ₃ N ₃₆ O ₁₄ Pd ₃ , 2054.14
Crystal system	Triclinic (<i>P</i> -1)
<i>a</i> / Å	10.5209(4)
<i>b</i> / Å	13.7690(9)
<i>c</i> / Å	16.456(10)
α / °	107.486(6)
β / °	108.070(4)
γ / °	96.178(4)
<i>V</i> / Å ³	2110.3(2)
ρ_{calc} / Mgm ⁻³	1.616
data/restraints/parameters	8023/0/553
<i>R</i> (<i>F</i>) { <i>I</i> >2 σ (<i>I</i>), all} / %	0.0929(0.2563)
<i>R</i> _w (<i>F</i> ²) { <i>I</i> >2 σ (<i>I</i>), all} / %	0.1036(0.2619)
GoF	1.092

Table S3. Selected structural parameters for 1 ^{Pt}					
Temperature /K	240	192	170	120	90
Spin State, HS ⁿ LS ¹⁻ⁿ	HS ^{1.0} LS ^{0.0}	HS ^{0.833} LS ^{0.167}	HS ^{0.667} LS ^{0.333}	HS ^{0.167} LS ^{0.833}	HS ^{0.0} LS ^{1.0}
< <i>d</i> _{Fe1(a)-N} > /Å ^[a]	2.162(2)	2.144(4)	2.147(2)	2.012(2)	1.989(8)
< <i>d</i> _{Fe1(b)-N} > /Å ^[a]	-	2.114(6)	2.102(6)	-	-
< <i>d</i> _{Fe2(a)-N} > /Å ^[a]	2.148(4)	2.030(2)	1.963(2)	1.956(7)	1.955(2)
< <i>d</i> _{Fe2(b)-N} > /Å ^[a]	-	2.117(2)	2.140	-	-
$\Sigma_{\text{Fe1(a)}} / ^{\circ}$ ^[b]	18	17.6	26.4	23.6	24.8
$\Sigma_{\text{Fe1(b)}} / ^{\circ}$ ^[b]	-	23.3	20.8	-	-
$\Sigma_{\text{Fe2(a)}} / ^{\circ}$ ^[b]	20.1	13.1	10.7	12.3	12.1
$\Sigma_{\text{Fe2(b)}} / ^{\circ}$ ^[b]	-	18.4	20.5	-	-
Fe1(a)-N≡C/°	164.6-167.8	164.9-166.6	162.6-166.8	167.5-169.3	168.9-170.1
Fe1(b)-N≡C/°	-	163.1-165.0	164.5-165.8	-	-
Fe2(a)-N≡C/°	173.1-177.2	173.3-179.3	174.3-179.5	172.9-179.3	172.9-178.6
Fe2(b)-N≡C/°	-	173.7-176.1	173.8-177.8	-	-
[a] Average Fe-N distance. [b] Octahedral distortion parameter calculated by sum of 90- θ for the twelve <i>cis</i> -N-Fe-N angles in the octahedron.					

Table S4. Structural parameters of 1^{Pd}			
Temperature/K	230	Temperature/K	230
$\langle d_{\text{Fe1-N}} \rangle / \text{\AA}$	2.144	host...guest	
$\langle d_{\text{Fe2-N}} \rangle / \text{\AA}$	2.149	N12...O4	3.652
$\sum^{\text{Fe1}} / ^\circ$	21.2	N16...O6	2.779
$\sum^{\text{Fe2}} / ^\circ$	19.3	C7...O7	3.652
Fe1-N \equiv C	166.2-169.0	N12...O7	2.929
Fe2-N \equiv C	172.8-177.8	O3...O7	2.835
		O2...O6	3.251
		O1...O4	2.833
		O5...O1	2.666
		host...host	
		C25...O2	3.260
		C23...O3	3.369
		guest...guest	
		O4...O5	2.718
		O5...O6	2.766

Table S5. Hydrogen bonding interaction distances (Å) for 1^{Pt}			
Temperature /K	240	120	90
host...guest			
N12...O4	3.679	3.602	3.581
N16...O6	2.777	2.749	2.745
C7...O7	3.656	3.497	3.482
N12...O7	2.942	2.841	2.847
O3...O7	2.838	2.756	2.763
O2...O6	3.265	3.230	3.217
O1...O4	2.818	2.756	2.754
O5...O1	2.651	2.593	2.602
host...host			
C25...O2	3.253	3.222	3.204
C23...O3	3.397	3.260	3.248
guest...guest			
O4...O5	2.716	2.664	2.665
O5...O6	2.772	2.743	2.743

Table S6. Hydrogen bonding interaction distances (Å) for 1 ^{Pt}		
Temperature/K	192	170
host...guest		
O3...O10	2.769	2.761
O5...O9	2.648	2.635
O6...O12	2.773	2.807
O2...O13	2.804	2.832
O1...O7	3.356	3.395
O5...O8	2.806	2.785
N22...O11	2.783	2.753
N18...O14	2.764	2.771
N14...O12	3.667	3.600
N26...O13	2.922	2.898
host...host		
O3...C20	3.352	3.285
O1...C31	3.280	3.283
O4...C23	3.321	3.228
O2...C47	3.358	3.363
guest...guest		
O7...O8	2.743	2.716
O7...O11	2.750	2.819
O12...O9	2.678	2.697
O10...O12	2.882	2.838

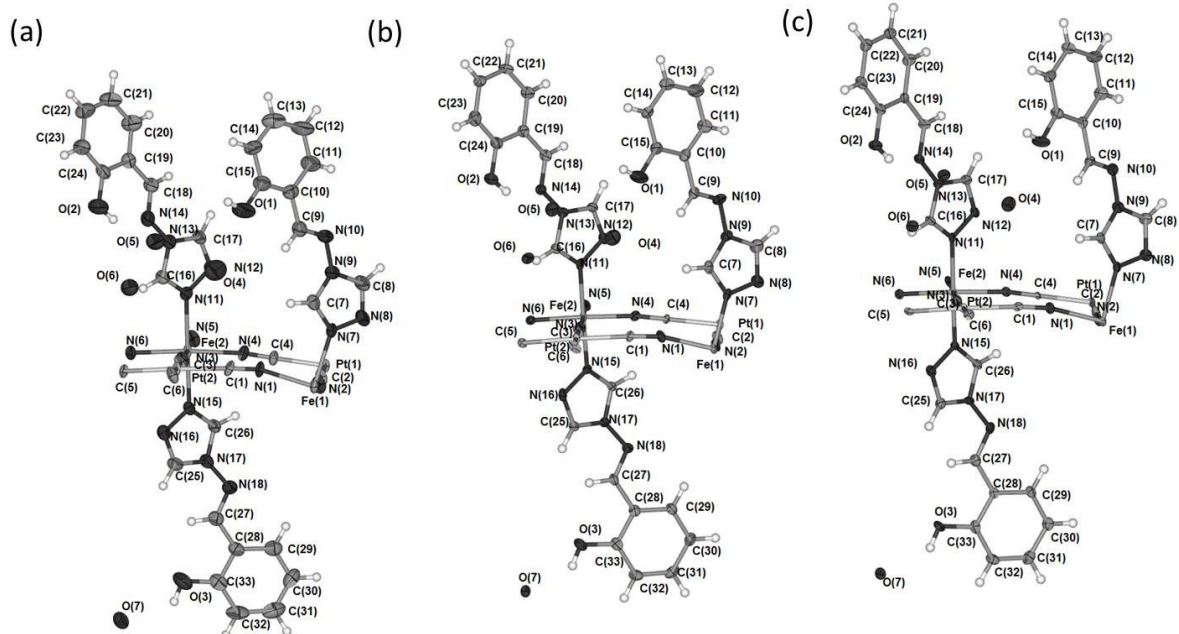


Figure S2. ORTEP structure representation (50% probability) of 1^{Pt} at (a) 240 K, (b) 120 K and (c) 90 K.

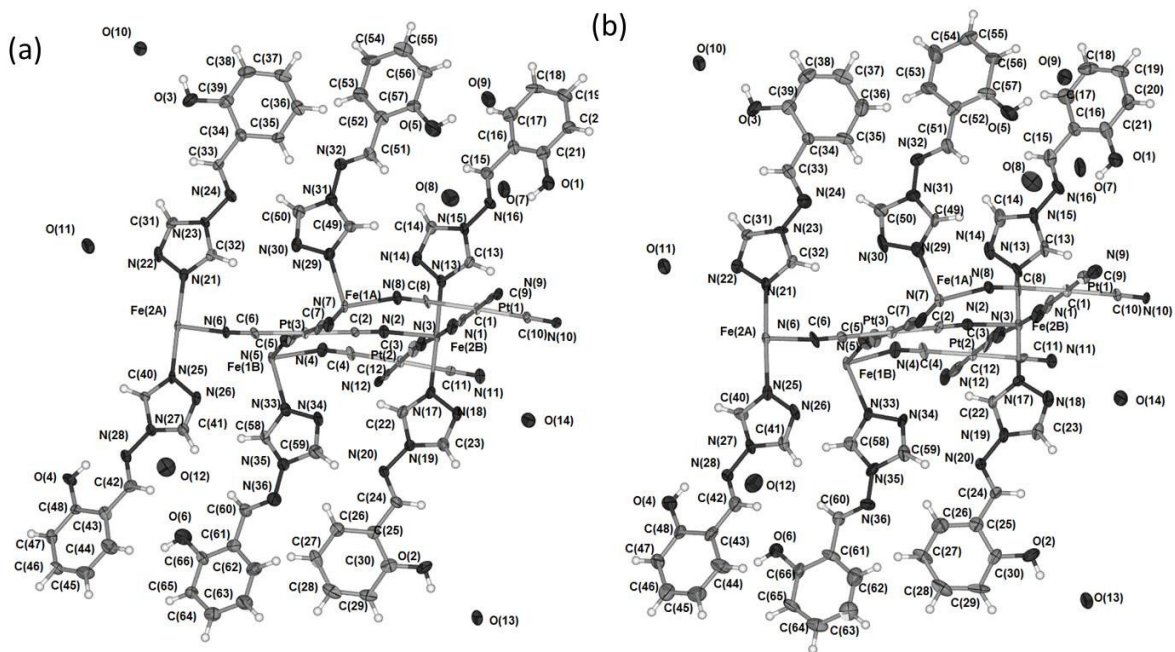


Figure S3. ORTEP structure representation (50% probability) of 1^{Pt} at (a) 170 K and (b) 192 K.

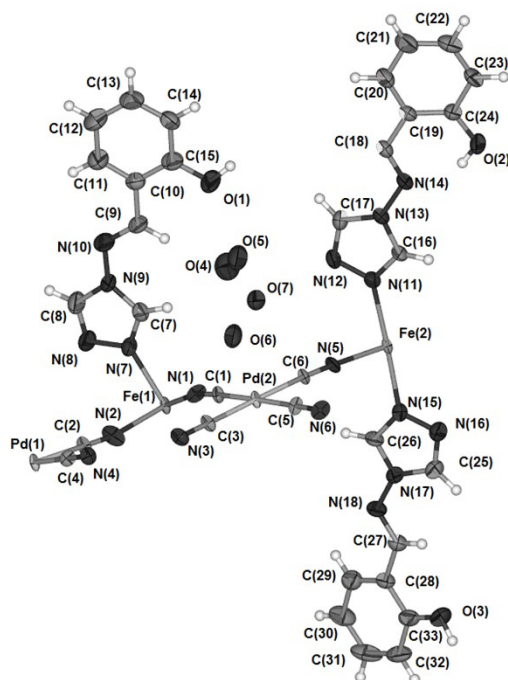


Figure S4. ORTEP structure representation (50% probability) of 1^{Pd} at 230 K.

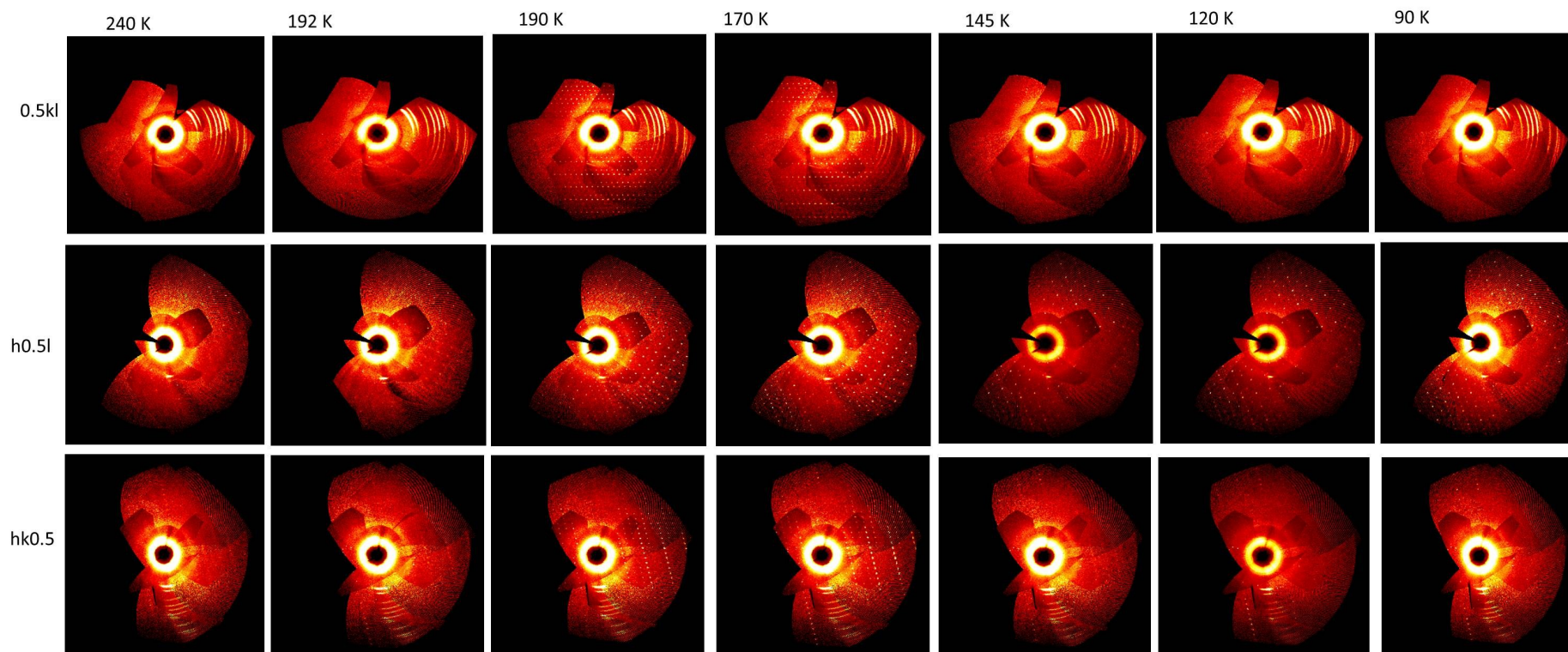


Figure S5. Variable temperature precession images for 1^{Pt} at $(0.5kl)$, $(h0.5l)$ and $(hk0.5)$ (based on the parent cell) showing the emergence of new reflections at 192 and 170 K, which are absent at other temperatures. We note that the reflections apparent in the $(h0.5l)$ orientation at all temperatures (but most intense in the 190 and 170 K temperatures due to the phase transition) are indicative of a doubling of the b -axis parameter. The high degree of pseudo symmetry in this doubled cell prevented unambiguous determination of the modulated structure; we note here that the presence of these reflections may indicate that additional long-range ordering between layers may exist.

S3 Powder X-ray diffraction

Polycrystalline samples of **1^{Pd}** and **1^{Pt}** were ground as a slurry and loaded into a quartz capillary (0.7 mm diameter), which was sealed to prevent solvent loss. The X-rays (17.03 keV, 0.72808 Å) available at the 17-BM beamline at the Advanced Photon Source at Argonne National Laboratory were used in combination with a Perkin Elmer area detector with a carbon window to record diffraction patterns. The sample temperature was controlled using an Oxford Cryosystems open flow cryostat, and the data were collected in 20 s exposures upon continuous ramping over the range 300 – 100 K, at 120 K h⁻¹. This corresponds to the collection of diffraction images at 2 K intervals. The raw images were processed using Fit-2D.⁷ LaB₆ was used as a standard. Le Bail analyses of the diffraction data were performed within TOPAS.⁸ Figure S6 shows the unit cell parameter evolution versus temperature for **1^{Pt}** compared to the magnetic data over the same temperature range.

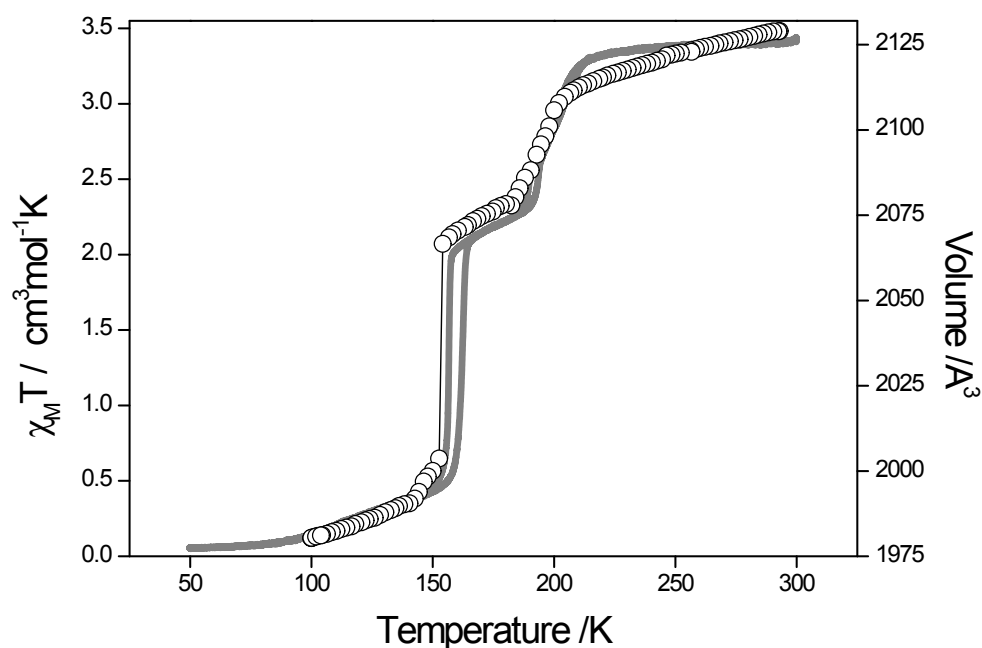


Figure S6. Variable temperature unit cell evolution extracted from Le Bail refinement of individual powder X-ray diffraction patterns (o) for **1^{Pt}**. Plotted with comparison to magnetic susceptibility data (grey line) to show overall match.

S3. Magnetic Susceptibility Measurements

Temperature dependent magnetic susceptibility

Data for 1^{Pd} and 1^{Pt} were collected on a Quantum Design Versalab Measurement System with a Vibrating Sample Magnetometer (VSM) attachment. Measurements were taken continuously under an applied field of 0.3 T over the temperature range 300 - 50 - 300 K, at a ramp rate of 2 K min^{-1} . The samples were additionally measured using a range of scan rates (0.5 – 4 K min^{-1}) with no obvious variation in magnetic behavior; thus, only the 2 K min^{-1} data are presented.

Light-induced magnetic susceptibility

Photomagnetic measurements were performed on 1^{Pd} using a set of photodiodes coupled via an optical fiber to the cavity of a MPMS-5S Quantum Design SQUID magnetometer operating at 2 T. Samples were prepared in a thin layer (~ 0.1 mg) to promote full penetration of the irradiated light.⁹⁻¹⁰ Irradiation to photo-saturation was carried out ($\lambda = 510$ nm) then irradiation was ceased and the temperature increased at a rate of 0.3 K min^{-1} to 100 K. The magnetisation was measured every 1 K to determine the $T(\text{LIESST})$ value, which was determined as being the extreme of the $\delta\chi_M T / \delta T$ versus T curve (Figure S2).⁹⁻¹¹ The $T(\text{LIESST})$ value describes the limiting temperature above which the light-induced magnetic high-spin information is erased in a SQUID cavity. In the absence of irradiation, the magnetic susceptibility was also measured over the temperature range 10 – 300 K to follow the thermal spin transition and to obtain a low temperature baseline. In addition, reverse LIESST measurements were performed by first attaining complete photo-saturation by irradiation of the sample at 10 K, then irradiating with 830 nm light. Figure S7 shows the LIESST properties of 1^{Pd} .

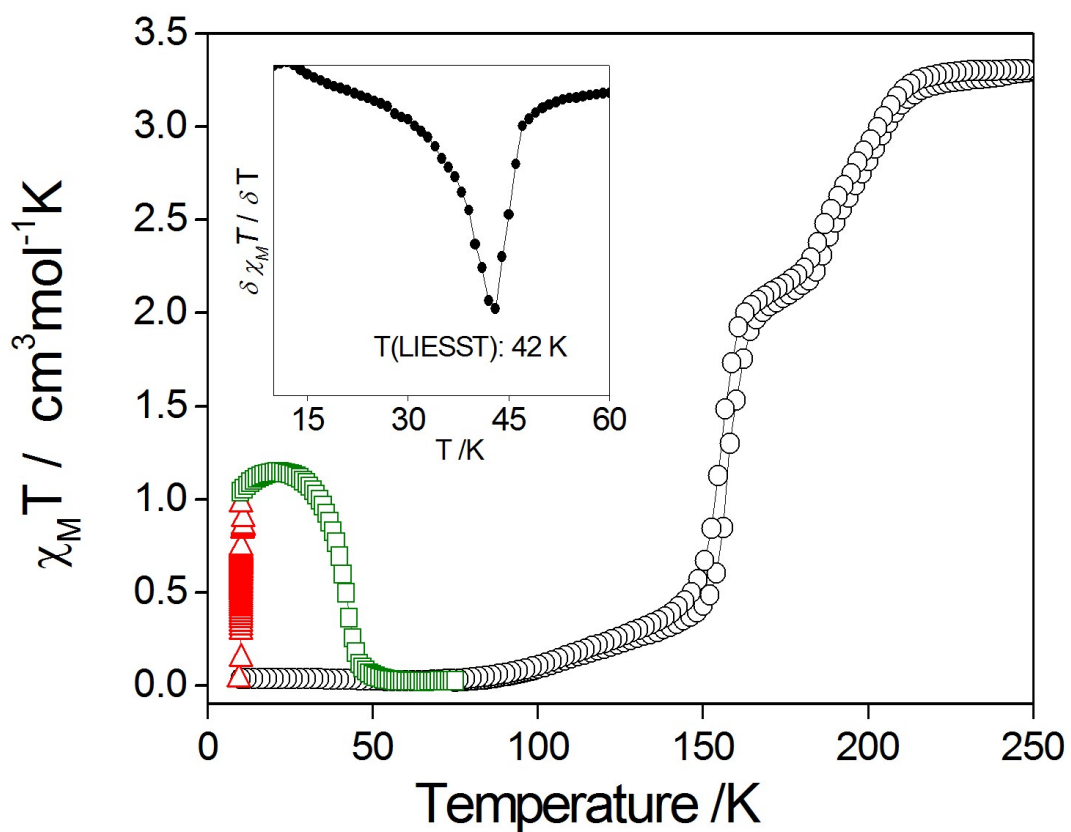


Figure S7. $\chi_M T$ versus temperature for 1^{Pd} (black (o): thermal spin transition, red (Δ): irradiation at 10 K with $\lambda = 532$ nm and green (\square): relaxation in the dark showing photo-excitation properties. Inset: derivative of relaxation versus temperature revealing a LIESST value of 42 K.

References

- [1] *APEX II Software Package* 2005, Madison, WI., Bruker AXS Inc. .
- [2] *CrysAlisPro* Agilent Technologies XRD Products Oxfordshire.
- [3] *SMART, SAINT and XPREP. Area detector and data integration and reduction software* 1995, Bruker Analytical Instruments Inc. Madison, Wisconsin, USA.
- [4] G. M. Sheldrick, *SADABS. Empirical adsorption correction program for area detector data* 1996, University of Gottingen, Germany.
- [5] *SHELXL97. Program for crystal structural solution and refinement* 1997, Madison Wisconsin, Bruker Analytical Instruments Inc.
- [6] L. J. Barbour, X-SEED University of Stellenbosch, South Africa, 1999.
- [7] A. P. Hammersley, *J. Appl. Cryst.* 2016, 49, 646-652.
- [8] *TOPAS v 4.2* 2009, Bruker ASX.